

Spiral-like structure in nearby clusters of galaxies

T. F. Laganá¹, F. Andrade-Santos¹, and G. B. Lima Neto¹

Universidade de São Paulo, Instituto de Astronomia, Geofísica e Ciências Atmosféricas, Departamento de Astronomia, Rua do Matão 1226, Cidade Universitária, 05508-090, São Paulo, SP, Brazil.

Received 25 August 2009 / Accepted 17 November 2009

ABSTRACT

Context. X-ray data analysis have recently revealed fairly complex structures in cluster centres to be more common than expected. Besides, great part of these structures resemble in morphology, presenting a spiral-like substructure.

Aims. It is not yet well known how this specific pattern is formed or maintained. In particular, understanding the nature of these spiral-like feature at the centre of some clusters is the major motivation of this work.

Methods. We analyse *Chandra* deep observation data of 15 nearby galaxy clusters ($0.01 < z < 0.06$). We used X-ray temperature and substructure maps to detect small features in the core of the clusters.

Results. We detect a spiral-like feature in the centre of 7 clusters: A85, A426, A496, Hydra A cluster, Centaurus, Ophiuchus and A4059. This particular pattern is similar to those found in numerical hydrodynamic simulations of cluster merger with non-zero impact parameter. In some clusters of our sample a strong radio source also occupies the inner region of the cluster, suggesting a possible connection between the two. Our investigation lends support to the fact that these spiral-like structures are due to off-axis minor mergers. Since these features are regions of high density they may confine radio emission from the central galaxy producing, in some cases, unusual radio morphology.

Key words. Keywords should be given

1. Introduction

Previous studies have shown that many clusters are still in the process of forming, with groups or individual galaxies falling down from the outer large scale structure filaments (e.g., Durret et al. 2003). Moreover, temperature maps of the X-ray emitting gas have shown that even clusters with apparently relaxed structures in X-ray could have perturbed temperature maps, revealing recent ongoing mergers (e.g., Finoguenov et al. 2005; Durret & Lima Neto 2008). The evidence of these small structures is one of the main achievements of the present era of X-ray telescopes such as *Chandra* and *XMM-Newton*. However, the presence of cooling-cores suggest that recent merger(s) have not had time to destroy the cooling-core.

More than 70% of cooling-flow clusters contain a central cD galaxy with radio source (e.g., Burns 1990; Eilek 2004). *Chandra* observations of these systems have revealed that the core of many clusters present morphological complexities that are thought to arise from the interaction between the intra-cluster medium (ICM) and the central radio galaxy.

The most important connection between X-ray ICM and the non-thermal relativistic electrons that produce the radio emission is dynamical. In the case of very energetic

jets, the ICM is heated and compressed due to supersonic shocks (Heinz et al. 1998; Reynolds et al. 2001). However, there are weaker jets that do not lead to an efficient shock heating, but it produces a bubble of low-density gas, which are identified as depressions in the X-ray surface brightness, that rise due to buoyancy (e.g., Churazov et al. 2001; Brüggén & Kaiser 2002; McNamara et al. 2005).

On the other hand, the ICM can also affect the radio emission from radio galaxies putting boundaries to the radio emission. It has been reported the unusual radio morphology of central cluster galaxies that fill X-ray cavities of low density (Boehringer et al. 1993; Taylor et al. 1994; Fabian et al. 2000, 2002; Taylor et al. 2002). The most extreme case of radio distortion is the amorphous radio galaxy PKS 0745-191 in the core of the Centaurus cluster (Taylor et al. 1994).

Another interesting feature that has been reported recently is the spiral-like feature present in the core of Perseus (Churazov et al. 2003; Fabian et al. 2000; Taylor et al. 2002), A2204 (Sanders & Fabian 2008) and A2029 (Clarke et al. 2004). This spiral pattern was also found in hydrodynamical simulations of merging clusters with nonzero impact parameters (Gómez et al. 2002; Ascasibar & Markevitch 2006). When the infalling sub-

cluster passes through the cluster centre, it causes a disturbance in the mass peak. Thus, the central cool gas of the main cluster acquires angular momentum, resulting in a spiral pattern.

To better understand the ICM-radio interaction and to characterize the nature of the spiral feature, we present a sample of 15 nearby clusters, among which 7 present this feature in the temperature and in the substructure maps, a high cooling-flow and a radio galaxy embedded in it. To do so, the paper is organized as follows: in Sect. 2 we describe the data sample and the *Chandra* data analysis, in Sect. 3 we explain the image procedures used to detect the spiral-like pattern, in Sect. 4 we present the results and the notes on individual clusters, in Sect. 5 we discuss a possible scenario to explain the spiral-like feature formation and the ICM-radio connection, in Sect. 6 we present a synthetic image constructed to roughly mimic the surface brightness of the Perseus cluster and in Sect. 7 we summarize our findings.

All distance-dependent quantities are derived assuming the Hubble constant $H_0 = 70 \text{ km s}^{-1} \text{ Mpc}^{-1}$, $\Omega_M = 0.3$ and, $\Omega_\Lambda = 0.7$.

2. Observation and Data Reduction

2.1. Cluster selection

The objects in our sample were drawn from a set of clusters within the redshift range $0.01 < z < 0.06$ and also with *Chandra* public data. Then we imposed clusters to have large exposure times, that is, of at least 35 ks. We ended up with 15 clusters which are presented in Tab. 1.

2.2. Chandra data reduction

In order to obtain calibrated images without artifacts, adequate to achieve our goal, it is necessary to follow a series of procedures, otherwise we would have contamination, which can be detected as substructures.

We have used the package CIAO 3.4. Initially a level 2 event files has been generated from a level 1 events file, using the standard procedure¹ and the latest calibration, CALDB 3.3.0. Periods with flares, that are high spurious counts caused by protons accelerated by the Sun, were excluded using the *lc_clean* script. At this point, a re-binned image with pixels corresponding to 16 raw physical pixels (4x4) is created from the new level 2 event file, in the energy band from 0.3 to 7.0 keV. Then, we produced exposure maps and use them to obtain flat images from which the source point are removed by filling circles around each source with random sampling with the same distribution as found in a circular region close to the source. Finally, we may fit a 2D analytical surface brightness model.

3. Imaging

As the bremsstrahlung emissivity depends on the temperature and surface brightness, irregularities can be detected either as temperature or as density discontinuities. As $\epsilon \propto T^{1/2} n^2$, these substructures are stronger in the surface brightness maps. Thus, to break the degeneration, we used substructure (which depends on the surface brightness distribution, Andrade-Santos et al. 2009) and temperature maps to analyse in details the inner parts of the clusters in our sample.

In Fig.2, we see that the X-ray emission is not symmetrically distributed around the cluster core, indicating the presence of a significant structure in the inner region of several clusters. To investigate this further, we compared these images with the temperature and the substructure maps.

3.1. X-ray substructures

We have developed a new method to quantify substructures in clusters of galaxies using 2D surface brightness fits. This method was tested for 47 galaxy clusters observed with *Chandra* (Andrade-Santos et al. 2009).

This method for quantifying and identifying substructures is based on the analysis of the number and intensity of (sub) structures detected by an algorithm of the type *friends-of-friends* (FOF). This analysis is done in a residual image, which is the result from the subtraction of the surface brightness model image, obtained by fitting a bidimensional analytical model (β -model or Sérsic) with elliptical symmetry (using Sherpa/CIAO, which fits a model minimizing the χ^2), from the cluster X-ray image. All surface brightness model parameters are free to vary, including the ellipticity, the position angle, the center, etc. In particular, for identifying substructures in this work, we used a threshold in the residual image to separate the pixels which had a number of counts statistically significant above or below the 2D fitted model surface brightness at that corresponding position. The threshold was defined as 3 times the local X-ray background variance. Once the pixels were separated, we identified these regions as substructure regions, using the FOF algorithm to link together the pixels above the threshold. This is a robust method if applied to observations with good signal/noise ratio, which is the case, since the clusters in our sample are rich objects at very low redshifts ($z < 0.06$) and were observed for more than 35ks.

3.2. Temperature maps

Ideally, one would prefer to compute a temperature map using spatially resolved spectroscopy as we did in Laganá et al. (2008). This, however, is very timing consuming. We opt for another approach, namely compute the hardness ratio maps and then converting it to a temperature map. Therefore, we are able to display significant

¹ <http://cxc.harvard.edu/ciao3.4/threads/createL2/>

Table 1: Observational informations

Cluster	RA (J2000)	DEC (J2000)	z	Detector	Exposure time (ks)	Soft band* (keV)	Hard band* (keV)	n_{H}^{\ddagger} (10^{20} cm^{-2})
Abell 85	00:41:37.80	-09:20:33.0	0.055	ACIS-I	38.91	0.3-1.4	1.4-6.0	2.78
Abell 426	03:19:48.20	+41:30:42.2	0.018	ACIS-S	98.20	0.3-1.4	1.4-6.0	13.6
Abell 496	04:33:37.00	-13:14:17.0	0.033	ACIS-S	76.08	0.3-1.3	1.3-6.0	3.78
Abell 3376	06:02:10.00	-39:57:21.0	0.046	ACIS-I	44.85	0.3-1.5	1.5-6.0	4.58
Abell 754	09:09:09.00	-09:39:39.0	0.054	ACIS-I	44.77	0.3-1.5	1.5-6.0	4.82
Hydra A	09:18:05.70	-12:05:42.5	0.013	ACIS-S	100.13	0.3-1.2	1.2-6.0	4.60
Centaurus	12:48:48.90	-41:18:44.4	0.011	ACIS-S	90.19	0.3-1.2	1.2-6.0	8.56
Abell 1644	12:57:33.00	-17:20:28.0	0.047	ACIS-I	52.17	0.3-1.6	1.6-6.0	4.11
Abell 1991	14:54:31.50	+18:38:32.0	0.059	ACIS-S	38.81	0.3-1.1	1.1-6.0	2.46
Abell 2052	15:16:44.50	+07:01:16.6	0.035	ACIS-S	128.63	0.3-1.2	1.2-6.0	2.71
Abell 2107	15:39:39.00	+21:46:58.0	0.041	ACIS-I	36.04	0.3-1.5	1.5-6.0	4.45
Ophiuchus	17:12:27.80	-23:22:11.5	0.028	ACIS-S	51.18	1.3-4.0	4.0-7.0	40.0
Abell 3667	20:13:07.25	-56:53:24.0	0.056	ACIS-I	105.01	0.3-1.6	1.6-6.0	4.44
Abell 4059	23:57:00.70	-34:45:33.0	0.047	ACIS-S	93.34	0.3-1.2	1.2-6.0	1.21
Abell 2589	23:23:57.40	+16:46:39.0	0.041	ACIS-S	54.13	0.3-1.3	1.3-6.0	3.15

* Soft and hard bands used to construct the hardness ratio.

‡ Hydrogen column densities adopted to construct HR (Dickey & Lockman 1990).

small-scale features without resorting to a computer intensive method.

The hardness ratio (HR) maps, or color maps, are defined as the ratio between the fluxes in two different bands and they may be interpreted as a projected temperature map. They can be defined as [hard smoothed image - soft smoothed image] / [smoothed hard energy band image + smoothed soft energy band image]. These bands are specified for each cluster in Tab. 1 and they were chosen in order to have two bands with almost the same net counts.

We made use of the *csmooth* tool in *Chandra* Interactive Analysis of Observations (CIAO), an adaptive smooth algorithm, to bin the data using bins of large angular size in order to examine possible structures in the image. In adaptive binning, the size of the smoothing kernel changes over the original image to create a constant S/N per pixel in the output image. The hard and the soft energy band images were smoothed identically, with the same adaptive kernel, avoiding spurious artifacts and yielding meaningful hardness ratios.

To convert HR maps into temperature maps we require a simple algorithm to compare the relative fluxes in different X-ray bands to a theoretical plasma emission model. Thus, based on the assumption of a single temperature, the HR- kT relation was estimated for each cluster, and an example is shown in Fig. 1 for A496. Watanabe et al. (2001) has also used this procedure to construct the temperature map of Ophiuchus using ASCA data. To do so, we took into account the weighted response matrices (RMFs), effective area files (ARFs) generated with CIAO 3.4., exposure maps for each observation, the hydrogen column densities for each cluster (as specified in Table 2) and we adopted a fixed metallicity value of 0.35 for all clusters. In Fig. 1 we show that the HR conversion into plasma temperature presents little variation assuming different metallicity values.

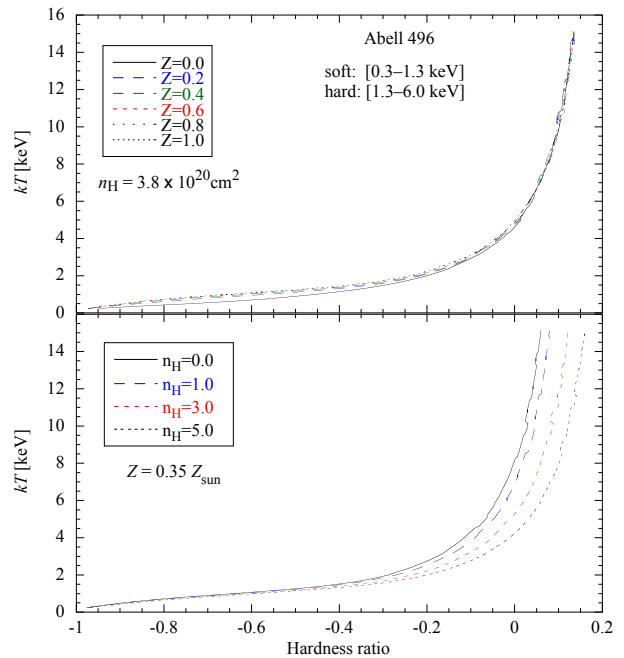


Fig. 1: Hardness ratio conversion into plasma temperature, using Abell 496 as an example. **Top:** HR to temperature conversion assuming different metallicity values (in solar units) and everything else fixed. **Bottom:** HR to temperature conversion assuming different hydrogen column densities (in 10^{20} cm^{-2}). While a metallicity error has an insignificant effect, n_{H} is important for an accurate determination of kT (in particular at high temperatures).

4. Results

We present in Fig.2 the X-ray images, temperature and substructure maps for the 15 clusters in our sample. In order to better investigate the properties of these clusters, we also present in Tab.2 the mean X-ray temperature, the

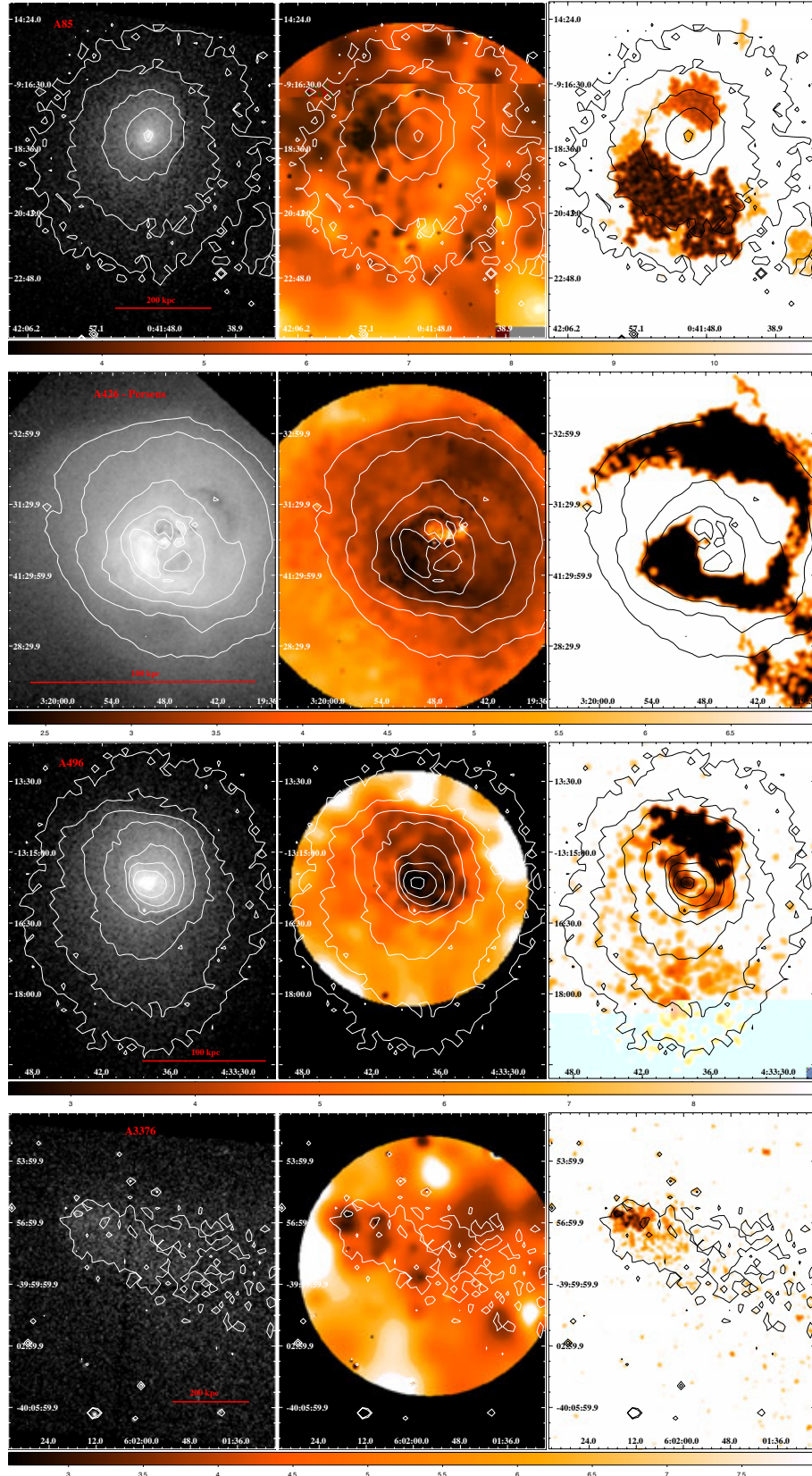


Fig. 2: Left panels: X-ray image; middle panel: temperature maps and right panels: substructure maps for A85, A426 (Perseus), A496, A3376. The color-bar gives the temperature in keV.

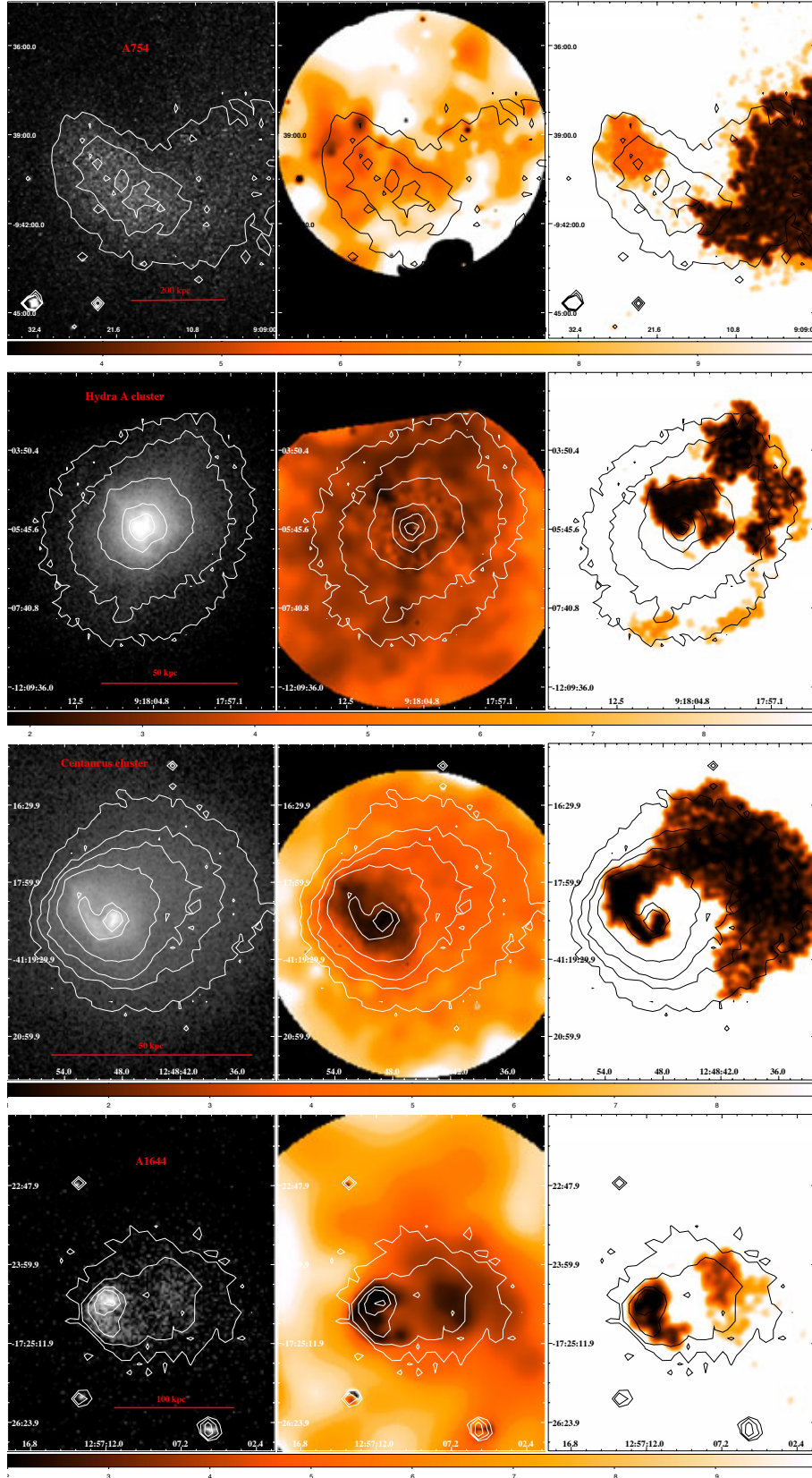


Fig. 2: *Cont.* Left panels: X-ray image; middle panel: temperature maps and right panels: substructure maps for A754, Hydra A cluster, Centaurus cluster and A1644. The color-bar gives the temperature in keV.

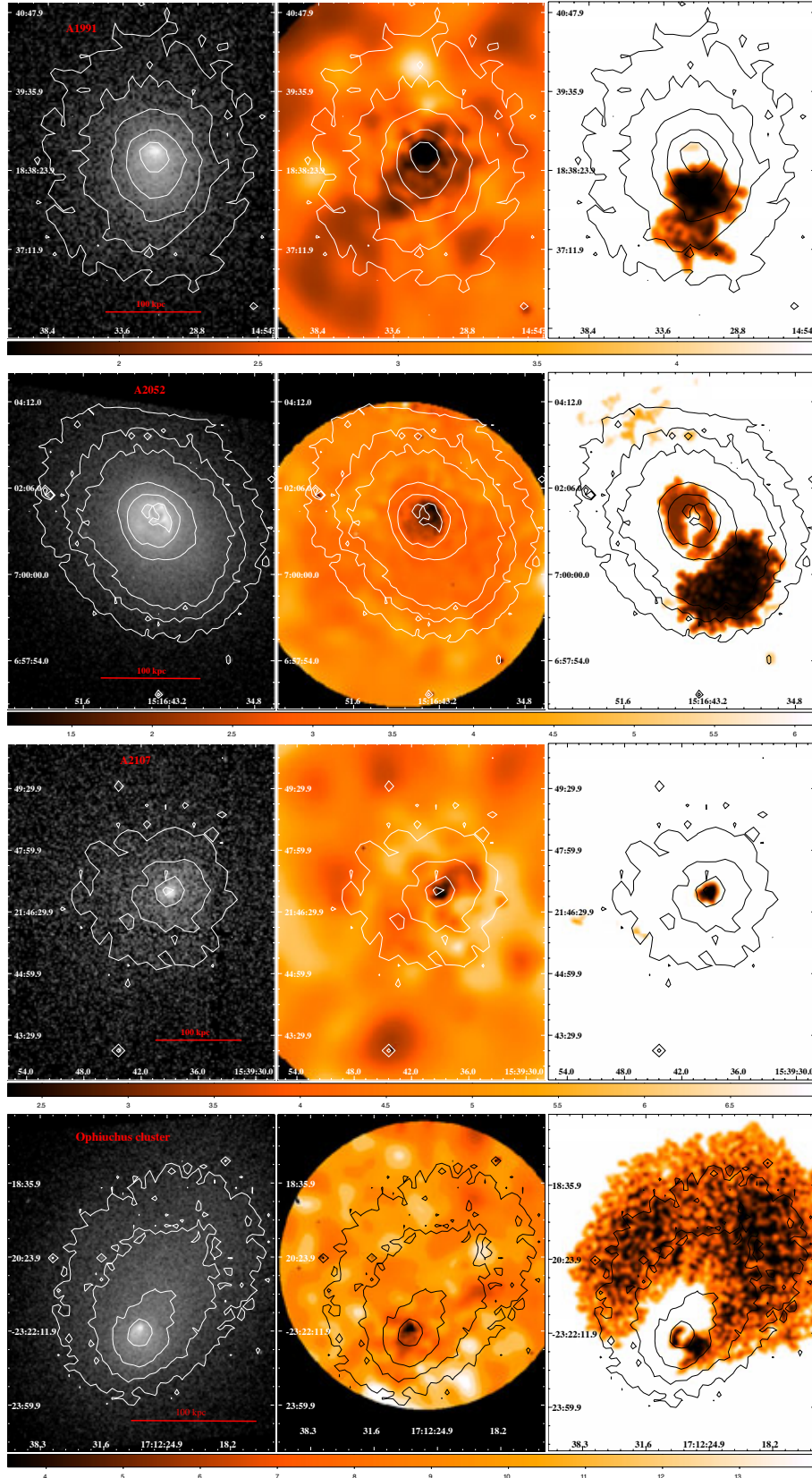


Fig. 2: *Cont.* Left panels: X-ray image; middle panel: temperature maps and right panels: substructure maps for A1991, A2052, A2107 and Ophiuchus cluster. The color-bar gives the temperature in keV.

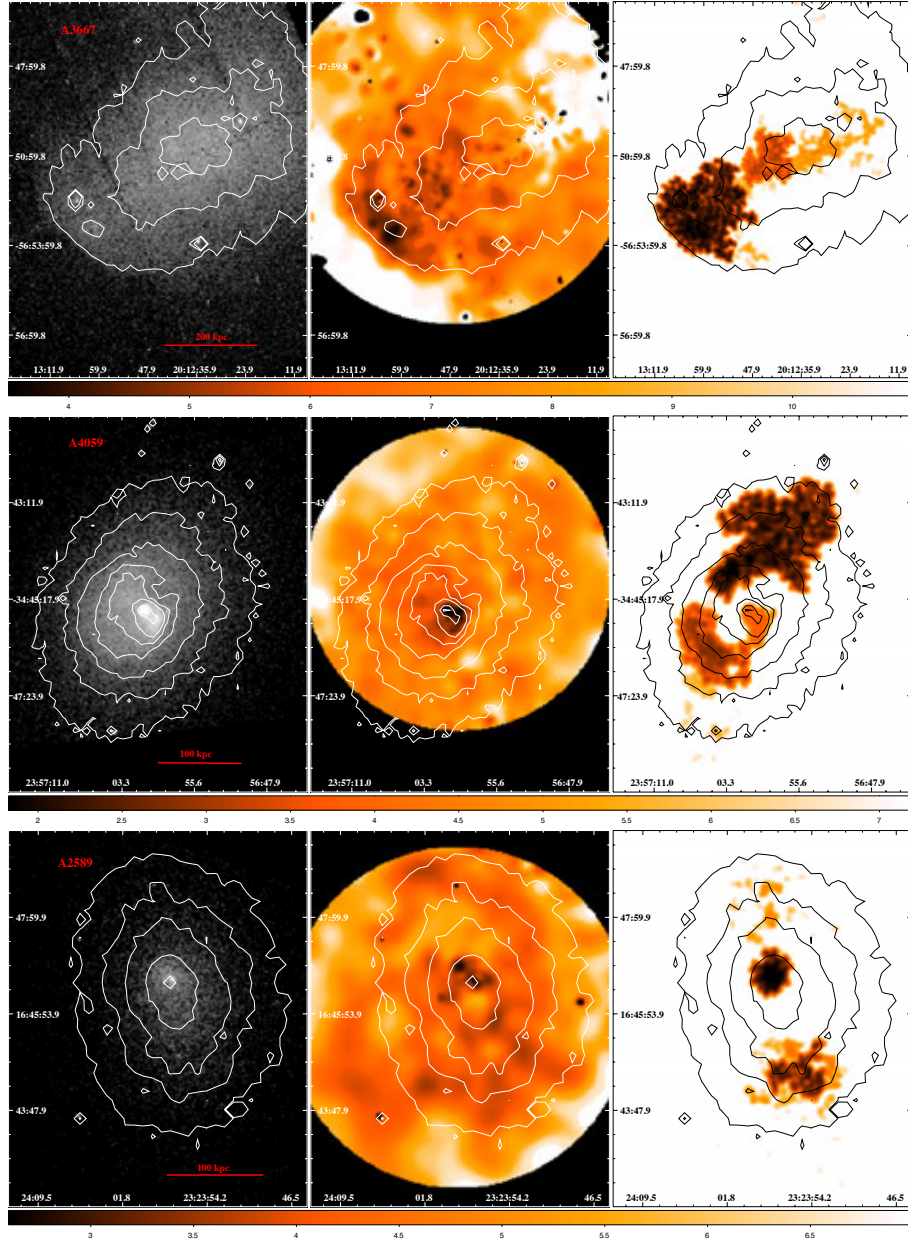


Fig. 2: *Cont.* Left panels: X-ray image; middle panel: temperature maps and right panels: substructure maps for A3667, A4059 and A2589. The color-bar gives the temperature in keV.

cooling-flow time and the X-ray luminosity obtained from the literature.

Although not clearly present in all temperature maps, a spiral-like structure in the inner part of 7 clusters (A85, A426, A496, Hydra A cluster, Centaurus, Ophiuchus and A4059) appears very clear in the substructure maps. These are the clusters with the highest cooling-flow rate and most of them are known to have a strong radio galaxy in the centre.

As the variations of temperature and density in shocks are positive correlated, the fact that this patterns are regions of low temperature and high density argues against strong shocks. Instead, these substructures resemble edges of cold fronts found in several clusters (e.g.,

Markevitch & Vikhlinin 2007; Dupke et al. 2007). Cold fronts can be directly related to cluster merger activities and comparing our results to numerical simulations (Gómez et al. 2002; Ascasibar & Markevitch 2006) one can see that the spiral-like features found here are morphologically similar to those found in the simulations. This indicate that its nature are dynamical and the possible scenario for its formation is discussed in Sect. 5.

Here, we also provide further information about each cluster in the sample, highlighting key aspects of previous studies.

Table 2: Cluster properties

Cluster	K. Arnaud [†]		Chen et al. (2007) [†]			Ikebe et al. (2002) [†]		Edge et al. (1992) [†]	
	kT (keV)	M ($M_{\odot} \text{ yr}^{-1}$)	kT (keV)	M ($M_{\odot} \text{ yr}^{-1}$)	L_X [0.1 – 2.4keV] ($h_{70}^{-2} 10^{44} \text{ erg/s}$)	kT (keV)	L_X [0.1 – 2.4keV] ($h_{70}^{-2} 10^{44} \text{ erg/s}$)	L_X [2 – 10keV] ($h_{70}^{-2} 10^{44} \text{ erg/s}$)	M ($M_{\odot} \text{ yr}^{-1}$)
Abell 85	6.8	128.5	$6.10^{+0.20}_{-0.20}$	200^{+33}_{-27}	13.54 ± 0.15	$6.51^{+0.16}_{-0.23}$	1.81 ± 0.02	10.56	236
Perseus (A426)	6.4	94.9	$6.79^{+0.12}_{-0.12}$	481^{+31}_{-32}	–	$6.42^{+0.06}_{-0.06}$	2.93 ± 0.04	15.40	183
Abell 496	5.7	100.7	$4.13^{+0.08}_{-0.08}$	114^{+35}_{-28}	5.28 ± 0.07	$4.59^{+0.10}_{-0.10}$	0.69 ± 0.01	3.56	112
Abell 3376	–	–	$4.30^{+0.60}_{-0.60}$	0^{+0}_{-0}	3.02 ± 0.07	$4.43^{+0.39}_{-0.38}$	0.74 ± 0.02	–	–
Abell 754	–	–	$9.00^{+0.50}_{-0.50}$	0^{+0}_{-0}	5.56 ± 0.15	$9.00^{+0.35}_{-0.34}$	4.0 ± 0.10	14.70	24
Hydra A	–	–	$3.80^{+0.20}_{-0.20}$	293^{+50}_{-84}	8.18 ± 0.06	–	–	3.89	315
Centaurus	2.3	31.3	$3.68^{+0.06}_{-0.06}$	24^{+6}_{-5}	1.67 ± 0.06	–	–	0.81	18
Abell 1644	5.1	19.3	$4.70^{+0.90}_{-0.70}$	0^{+0}_{-0}	5.49 ± 0.48	$4.70^{+0.90}_{-0.70}$	0.73 ± 0.06	3.33	19
Abell 1991	4.6	71.0	–	–	–	–	–	–	–
Abell 2052	3.7	30.8	$3.03^{+0.04}_{-0.04}$	108^{+188}_{-49}	3.32 ± 0.06	$3.12^{+0.10}_{-0.09}$	0.43 ± 0.01	1.97	90
Abell 2107	6.5	0.0	–	–	–	–	–	–	–
Ophiuchus	–	–	$10.26^{+0.32}_{-0.32}$	0^{+0}_{-0}	–	$10.25^{+0.30}_{-0.36}$	2.2 ± 0.07	21.28	75
Abell 3667	–	–	$7^{+0.60}_{-0.60}$	0^{+0}_{-0}	13.27 ± 0.15	$6.28^{+0.27}_{-0.26}$	1.78 ± 0.02	11.59	0
Abell 4059	–	–	$4.10^{+0.30}_{-0.30}$	69^{+20}_{-15}	3.92 ± 0.08	$3.94^{+0.15}_{-0.15}$	0.52 ± 0.01	2.65	124
Abell 2589	–	–	$3.70^{+2.20}_{-1.10}$	19^{+33}_{-19}	2.62 ± 0.06	$3.38^{+0.13}_{-0.13}$	3.44 ± 0.08	–	–

[†] All values were converted to a common cosmology with a Hubble constant given as $H_0 = 70 \text{ km s}^{-1} \text{ Mpc}^{-1}$.

4.1. Abell 85

A well-known subclump cluster, which also has a cold-front (Kempner et al. 2002) and is a merger candidate. The optical properties of this cluster shows evidence for galaxy star formation in the filament between the main cluster and the subclump (Boué et al. 2008), which is consistent with the previous hypothesis that the X-ray filament in Abell 85 is a gravitationally bound structure made of groups falling into the main cluster (Lima Neto et al. 2001; Durret et al. 2003).

From this work we clearly see a spiral-like structure on the substructure map. However, no correlation of this structure appears on the temperature map.

4.2. Abell 426 - Perseus

Churazov et al. (2003) presented XMM-Newton results, revealing a spiral-like structure in temperature and surface brightness maps. These authors concluded that this feature is possibly a contact discontinuity separating the main cluster gas from the gas of the infalling subcluster. A chain of galaxies is also associated with this region probably tracing the filament along which the merger started.

On the other hand, as it has a strong central radio galaxy, NGC 1275, Boehringer et al. (1993) argued that the thermal plasma was displaced by the inner parts of the radio lobe. In a more recent work Fabian et al. (2002) examined in detail the interaction of the radio source 3C84 with the surrounding medium, arguing that the inner lobes are currently expanding subsonically.

From our results one can see that this cluster is one of the clusters with a most prominent spiral-arm pattern in both temperature and substructure maps. The substructure found here is almost identical to the one detected by Churazov et al. (2003) (see their Fig. 7).

4.3. Abell 496

This cluster hosts a prominent cold-front (Dupke & White 2003), as sign of a recent minor merger, and although without much attention, a very prominent spiral-like pattern has already been presented in a previous work (Laganá et al. 2008) done with XMM-Newton data.

In Fig.2, a spiral-like feature is present in the substructure and in the temperature map. The pattern that appears in the temperature map is very similar in form to the one in A85.

4.4. Abell 3376

A nearby on-going merger cluster observed with *Suzaku* (Kawano et al. 2008) and with XMM-Newton (Bagchi et al. 2006). A non-thermal radio emitting structures at the outskirts of this cluster was found by these latter authors. They suggested that this structure probably traces the elusive shock waves of cosmological large scale matter flows.

4.5. Abell 754

A754 was one of the first clusters for which an X-ray temperature map was obtained from ROSAT data (Henry & Briel 1995) and from ASCA (Henriksen & Markevitch 1996), in which the gas velocity map (Evrard et al. 1996) already indicated the plume-like pattern. *Chandra* data analysis revealed a more complex merger geometry, possibly involving more than two subclusters (Markevitch et al. 2003). From XMM-Newton data, Kassim et al. (2001); Bacchi et al. (2003) confirmed this cluster as a major-merger cluster and also detected a plume-like feature at the centre. There is a diffuse radio source associated with this cluster (Henry et al. 2004).

In this work a large substructure is detected, but it does not present any particular shape.

4.6. A780 - Hydra A cluster

Fitchett & Merritt (1988) examined the dynamics of the Hydra cluster revealing that the velocity distribution of galaxies near the cluster centre is very flat. Although they did not suggest an infalling group scenario, they considered the importance of substructures in this cluster,

Chandra observations of the Hydra cluster reveal a feature in the X-ray surface brightness that surrounds radio lobes of the active galactic nucleus (AGN) at the cluster centre (Nulsen et al. 2005). These authors proposed that the shock front is driven by the expanding radio lobes and also the “new structure on smaller scales” is associated with the radio source. Wise et al. (2007) affirmed that the complex system found in this cluster was created by a continuous outflow or a series of bursts from the nucleus of the central galaxy. In this particular case, merger was not mentioned in the literature as a process to form this substructure.

From this work we see a truncated spiral-like feature in the substructure map that has a corresponding pattern of lower temperature.

4.7. Centaurus

To explain the particular morphology of this cluster, Churazov et al. (1999) based on ASCA imaging and spectral results, suggested that a subcluster centred on NGC 4709 is merging with the main cluster centred on NGC 4696.

Sanders & Fabian (2006) performed a detailed analysis of the core of the Centaurus cluster using a *Chandra* deep X-ray observation and XMM-Newton data. To explain the high metallicity present in the core of this cluster, the model proposed by these latter authors requires that the inner core of the Centaurus cluster has not suffered a major disruption within the past 8 Gyr, or even longer. In their temperature map the plume-like feature is present, although little attention was given to it. They also reported the discovery of ripple-like X-ray surface brightness oscillations in the core of this cluster of galaxies, explained as sound waves generated by the repetitive inflation of central radio bubbles.

From Fig. 2 one can see that this cluster has one of the most prominent spiral-like feature detected in the substructure map. The very inner region of this huge structure is also associated with a region of low temperature in the temperature map.

4.8. Abell 1644

This is a complex merging system observed with XMM-Newton, which is composed of a main cluster and a subcluster (Reiprich et al. 2004). These authors also detected a trail of cool, metal-rich gas closer to the subcluster. The combination of X-ray, optical and radio data results suggest that the subcluster has passed by the main cluster off-axis. Although temperature maps are presented in

their work, the plume-like feature is not resolved by XMM-Newton.

From our analysis, a discontinuous spiral-like feature is present in the substructure map. This pattern is not as evident as in Centaurus, Perseus and A85 but it in form it looks like the previous structures. Unfortunately, just the inner part of the substructure shows a correspondence with the temperature map.

4.9. Abell 1991

Sharma et al. (2004) analysed XMM-Newton data and detected an asymmetric surface brightness distribution with respect to the central galaxy. These authors detected bright knots of soft X-ray emission embedded in a cometary structure located northern of the optical centre of the cD galaxy. According to these authors, the knots have no obvious association with the radio source.

4.10. Abell 2052

Zhao et al. (1993) reported VLA results of radio source at the core of this cluster. More recently, Blanton et al. (2003, 2009) carried out a *Chandra* X-ray data analysis of large-scale properties of the cluster as well as the central region, which includes a radio source, presenting temperature and abundance profiles.

Two clear substructures are present in Fig.2 but they do not resemble to the other spiral-like feature presented in this work.

4.11. Abell 2107

Fujita et al. (2006) presented an analysis of *Chandra* observation of this cluster. Due to the fact that the cD galaxy has a large peculiar velocity and the ICM in the central region has an irregular structure, these authors concluded that this cluster is undergoing a merger.

From our results, A2107 presents the smallest substructure and an almost symmetric X-ray contours giving no direct evidence to a recent merger scenario.

4.12. Ophiuchus

Ophiuchus is one of the hottest X-ray cluster located 12 deg from the Galactic centre (Fujita et al. 2008). Using ASCA data, Matsuzawa et al. (1996) obtained image in the energy range of 0.7-10 keV showing that the peak of X-ray surface brightness is coincident with the cD galaxy. Later, Watanabe et al. (2001) presented temperature and metallicity profiles obtained with ASCA, with no signs of the plume-like feature. In their analysis, the ROSAT archival data suggest an ongoing merger, but *Chandra* image indicates that this cluster has a cool-core that is still undisturbed. Thus, if there is an ongoing merger it has to be a minor merger (e.g., Watanabe et al. 2001).

From the results presented in Fig.2, Ophiuchus is the cluster with the most prominent spiral-like pattern present in the substructure map. However, no significant feature was detected in the temperature map.

4.13. Abell 3667

This cluster has a double radio halo outside the central region (Rottgering et al. 1997; Markevitch et al. 1999). The galaxy distribution is bimodal (Proust et al. 1988), with the main component around the cD galaxy. A more recent multiwavelength study confirmed its merging nature based on *Chandra* and optical data (Owers et al. 2009a). Its X-ray image shows a clear cold front.

4.14. Abell 4059

Heinz et al. (2002) affirmed that there are clear signs of interaction between the radio galaxy and the ICM. However, these authors did not find a one-to-one correspondence between the radio lobes and the X-ray cavities (Heinz et al. 2002). Huang & Sarazin (1998) argued that it is likely that the radio plasma from the cD galaxy may have displaced the X-ray gas and created the X-ray cavities.

On the other hand, Choi et al. (2004) analysed various scenarios concluding that the most probable picture is a compression front associated with ICM bulk motion.

Reynolds et al. (2008) analysed a *Chandra* deep observation, revealing a subtle discontinuity in the gradient of the surface brightness that is approximately semi-circular in form and centred on the radio galaxy. The previous *Chandra* observations reported by Heinz et al. (2002) and Choi et al. (2004) had insufficient signal to detect this feature. Although it cannot be rigorously proved, Reynolds et al. (2008) interpreted this feature as a weak shock due to the radio galaxy activity. Such shocks are seen in all hydrodynamic simulations of jet/ICM interactions (Heinz et al. 2002; Vernaleo & Reynolds 2006, e.g.).

In this work, we show that this cluster has also a spiral-like substructure. The inner part of this pattern is linked to a region of lower temperature, as it is seen in the temperature map of Fig.2.

4.15. Abell 2589

The hot gas in the core region of A2589 is undisturbed by interactions with a central radio source (Buote & Lewis 2004). Except for a 16 kpc shift of the X-ray centre, A2589 possesses a remarkably symmetrical X-ray image (Zappacosta et al. 2006).

5. Discussion

The literature contains detailed studies of a large number of clusters with the larger cooling rates and a very powerful radio galaxy, e.g., Hydra A

(McNamara et al. 2000; David et al. 2001), Perseus (Fabian et al. 2000; Churazov et al. 2003) and the Centaurus cluster (Taylor et al. 1994). There is a correlation between radio emission by the central galaxies and the presence of cooling-flow that is known since Burns et al. (1981) and Jones & Forman (1984). The cooling gas is driven to a massive object in the central galaxy that might produce the radio emission. However, what is quite surprising is that the clusters that present well defined spiral-like structures are the ones with the larger cooling-flows (see Tab. 2) and with a powerful radio galaxy. The only exception is A2052 that does have an AGN (Blanton et al. 2003, 2009) and does not present a spiral-like substructure.

The presence of a strong cooling-flow and a powerful central radio galaxy indicates that its radiation has not yet had time to heat the surrounding gas of the inner parts of the clusters. This fact can be understood if we think about a cycle in which the cool gas feeds the central AGN that starts to heat the surrounding gas. While the central gas is not sufficiently heated and the cooling-flow is not suppressed, there will be a stage where both the AGN and the cool gas will coexist.

The radio morphology of some of these clusters that present spiral-like patterns appears quite different from the most radio galaxies in the sense that they fill the X-ray cavities (regions of low density). Taylor et al. (2002) showed that the eastern lobe of the central radio galaxy of Centaurus cluster appears to fill in the region bounded by the spiral-like structure, while the western lobes turn around it. Similar confinement has been found for other radio galaxies embedded in dense ICM. For example, radio emissions filling X-ray cavities were found in the core of Perseus cluster (Boehringer et al. 1993; Fabian et al. 2000, 2002), A2029 (Taylor et al. 1994) and Hydra A cluster (A780) (McNamara et al. 2000).

The ICM of merging clusters presents a variety of signatures of mergers such as cold-fronts and bow shocks. Although the most prominent cold fronts are produced in major mergers, cold fronts arising from minor mergers are expected to be much more frequent. Minor mergers generate subsonic turbulent gas motions within the cluster without destroying the cool-core. Different morphological features can arise from minor mergers, such as comet-like tails, bridges, plumes and edges (Poole et al. 2006). Thus, one possibility for the origin of this particular spiral excess found in 7 clusters of our sample is that they are the latter signature of a small galaxy cluster or group merging with the main one.

In a high-resolution numerical simulation of idealized cluster mergers, Ascasibar & Markevitch (2006) concluded that if an infalling subcluster has nonzero impact parameter, the cool gas of the main cluster acquires angular momentum, resulting in a spiral-like feature of cold front due to the gas sloshing. In their simulation, after 1.9 Gyr (see their Fig. 7) one can see a spiral-like pattern, in the gas density and temperature distribution, that are

morphologically similar to the structure found here. As they used a mass ratio of 1:5, the cool-core is preserved.

In a similar work, the numerical simulations of Gómez et al. (2002) can also mimic the results found here. In their merger 7, the subcluster has a small gas fraction and they assume a mass ratio of 1:16 so that the cooling-flow is not disrupted during the merger. An alternative explanation for the spiral-like structure is a contact discontinuity separating the main cluster gas from the gas of the infalling subcluster. However, it is also possible that the gas from the infalling subcluster is stripped out far from the core, never reaching the inner region of the main cluster (Churazov et al. 2003). In this way, the observed structure is composed only by the disturbed gas of the main cluster. A metallicity analysis can distinguish between the above scenarios. If the cold gas in the spiral-like pattern is a result from the main cluster gas sloshing, the metallicity in this region should be equal to the metallicity in the inner part of the main cluster. On the other hand, if it is a gas discontinuity, the metallicity in the spiral arm would be different from the inner part of the main cluster. The ICM enrichment analysis for this sample will be presented in a forthcoming work.

It is more likely that, in a scenario of a minor merger, the cooling-flow continue to feed the central galaxy which is turned on. Then, the radio emission will permeate the regions of low density, that is, they are going to fill the X-ray cavities being confined by the spiral-like feature. The effects of the ICM on the radio emission will be its distortion, giving rise to confined radio morphologies, as it is seen in some clusters.

It is worth noting that the spiral-like feature found here is not limited for the clusters in our sample but it was also found in other clusters, such as A1975 (Fabian et al. 2001), A262 (Blanton et al. 2004), A2029 (Clarke et al. 2004), A5098 (Randall et al. 2009), A1795 (Liuzzo et al. 2009) and A1201 (Owers et al. 2009b). More recently, this kind of pattern has also been observed in galaxy groups (Gastaldello et al. 2007; Randall et al. 2009) showing that they are not particular to clusters.

Since we find a high number of clusters that present this particular pattern, it would be interesting to bolster these findings using numerical simulations. Namely, it would be instructive to study the frequency of off-axis merger halos as a function of redshift that produce a cool gas spiral-like pattern when adopting a mass ratio of 1:5 (Ascasibar & Markevitch 2006) and 1:16 (Gómez et al. 2002). Unfortunately, these measurements are beyond the scope of our investigation.

From the theoretical point of view, future numerical hydrodynamical simulations could detect the signature of cluster mergers to compare to recent observations. In this sense, statistical studies of cluster morphology and substructures would provide important constraints to models of structure formation and evolution of the observed cluster properties. Despite the large amount of available data, the dynamical evolution of ICM substructures is still poorly understood. Here we have studied in detail

15 nearby galaxy cluster highlighting a particular ICM substructure morphology.

6. Synthetic Image

In this section we present a synthetic image, created using the *cfitsio* routine (library of routines for reading and writing data files in the FITS data format). This synthetic image was constructed by adding multiple components in order to roughly mimic the Perseus cluster X-ray surface brightness. The synthetic image was the result of adding a 2D β -model, an exponential spiral pattern and two bubbles in the inner region of the cluster. The components and the result of their addition is seen in Fig. 3.

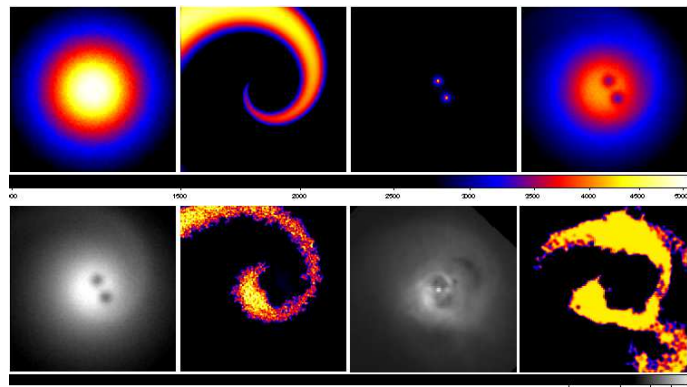


Fig. 3: Synthetic image constructed to roughly mimic the Perseus cluster X-ray surface brightness. Top panels from left to right: 2D β -model, exponential spiral pattern, two bubbles and the sum of these three components. Bottom panels from left to right: X-ray synthetic surface brightness, substructure map from this previous image, Perseus X-ray surface brightness and its substructure map.

The goal of generating this synthetic image is to follow the same procedures applied to the real clusters, of determining the substructures, and compare to the substructure of the Perseus cluster. Although clearly present, one can see that the spiral pattern is not highlighted in the synthetic surface brightness image (see top panel of Fig.3), which shows the importance of this method in finding structures that are hardly seen by eye.

The result obtained shows in the synthetic image substructure map a spiral-like pattern structure very similar to the one found in the Perseus clusters, reinforcing the detectability of these spiral-like patterns. Furthermore, the result shows that the Perseus cluster X-ray surface brightness and substructures can be apparently well described by the addition of three components, in particularly an exponential spiral-like pattern, similar to the one found in the results of numerical the simulation performed by Ascasibar & Markevitch (2006).

7. Conclusions

In the current scenario for the formation of structures, clusters of galaxies form hierarchically through mergers. Besides the modification of galaxy distribution and trigger the star formation, these merger events lead to variations of the physical properties, such as density and temperature variations that can be observed in X-rays. In this sense, the substructure maps have revealed to be a powerful technique to identify hidden structures that are the last record of the merger history.

In this paper we present 7 (A85, A426, A496, Hydra A cluster, Centaurus, Ophiuchus and A4059) out of 15 clusters that present a spiral-like substructure which are boundaries of cold-fronts and the cavities. The cavities inside these patterns are, in most of the cases, associated with a radio emission. The aim of this study is to highlight the frequency of this morphological type of pattern in nearby clusters. Our analysis shows how observational studies can improve the constraints on numerical simulations of structure formation and foster our understanding of ICM physical properties.

Comparing our results to numerical simulations (Ascasibar & Markevitch 2006), we discuss a model in which this spiral-like pattern is produced by an off-axis minor-merger that displace the central cool gas. As the minor merger do not disrupt the cool core, the central cool gas is still driven to the central object that may produce the radio emission. This radio emission is bounded by the ICM inhomogeneities that will probably produce overall radio appearance quite different from the most radio galaxies. Thus, we suggest that the distorted morphology of these radio emissions may be due to the confinement by the dense X-ray gas in the spiral pattern. However, our interpretation about the nature of the spiral-like pattern and its relation to X-ray cavities and radio emission is not further reinforced due to the lack of simulations that deal with merger signature.

Acknowledgements. The authors thank Florence Durret that triggered this work. The authors thank the anonymous referee for the suggestions. The authors also acknowledge financial support from the Brazilian agency FAPESP (grants: 2008/04318-7 and 2008/05970-0).

References

- Andrade-Santos, F., Lima Neto, G. B., & Laganá, T. F. 2009, Submitted to ApJ
- Ascasibar, Y. & Markevitch, M. 2006, ApJ, 650, 102
- Bacchi, M., Feretti, L., Giovannini, G., & Govoni, F. 2003, A&A, 400, 465
- Bagchi, J., Durret, F., Neto, G. B. L., & Paul, S. 2006, Science, 314, 791
- Blanton, E. L., Randall, S. W., Douglass, E. M., et al. 2009, ApJ, 697, L95
- Blanton, E. L., Sarazin, C. L., & McNamara, B. R. 2003, ApJ, 585, 227
- Blanton, E. L., Sarazin, C. L., McNamara, B. R., & Clarke, T. E. 2004, ApJ, 612, 817
- Boehringer, H., Voges, W., Fabian, A. C., Edge, A. C., & Neumann, D. M. 1993, MNRAS, 264, L25
- Boué, G., Durret, F., Adami, C., et al. 2008, A&A, 489, 11
- Brüggen, M. & Kaiser, C. R. 2002, Nature, 418, 301
- Buote, D. A. & Lewis, A. D. 2004, ApJ, 604, 116
- Burns, J. O. 1990, AJ, 99, 14
- Burns, J. O., White, R. A., & Haynes, M. P. 1981, AJ, 86, 1120
- Chen, Y., Reiprich, T. H., Böhringer, H., Ikebe, Y., & Zhang, Y.-Y. 2007, A&A, 466, 805
- Choi, Y.-Y., Reynolds, C. S., Heinz, S., et al. 2004, ApJ, 606, 185
- Churazov, E., Brüggen, M., Kaiser, C. R., Böhringer, H., & Forman, W. 2001, ApJ, 554, 261
- Churazov, E., Forman, W., Jones, C., & Böhringer, H. 2003, ApJ, 590, 225
- Churazov, E., Gilfanov, M., Forman, W., & Jones, C. 1999, ApJ, 520, 105
- Clarke, T. E., Blanton, E. L., & Sarazin, C. L. 2004, ApJ, 616, 178
- David, L. P., Nulsen, P. E. J., McNamara, B. R., et al. 2001, ApJ, 557, 546
- Dickey, J. M. & Lockman, F. J. 1990, ARA&A, 28, 215
- Dupke, R. & White, III, R. E. 2003, ApJ, 583, L13
- Dupke, R., White, III, R. E., & Bregman, J. N. 2007, ApJ, 671, 181
- Durret, F. & Lima Neto, G. B. 2008, Advances in Space Research, 42, 578
- Durret, F., Lima Neto, G. B., Forman, W., & Churazov, E. 2003, A&A, 403, L29
- Edge, A. C., Stewart, G. C., & Fabian, A. C. 1992, MNRAS, 258, 177
- Eilek, J. A. 2004, in The Riddle of Cooling Flows in Galaxies and Clusters of galaxies, ed. T. Reiprich, J. Kempner, & N. Soker, 165
- Evrard, A. E., Metzler, C. A., & Navarro, J. F. 1996, ApJ, 469, 494
- Fabian, A. C., Celotti, A., Blundell, K. M., Kassim, N. E., & Perley, R. A. 2002, MNRAS, 331, 369
- Fabian, A. C., Sanders, J. S., Ettori, S., et al. 2001, MNRAS, 321, L33
- Fabian, A. C., Sanders, J. S., Ettori, S., et al. 2000, MNRAS, 318, L65
- Finoguenov, A., Böhringer, H., & Zhang, Y.-Y. 2005, A&A, 442, 827
- Fitchett, M. & Merritt, D. 1988, ApJ, 335, 18
- Fujita, Y., Hayashida, K., Nagai, M., et al. 2008, PASJ, 60, 1133
- Fujita, Y., Sarazin, C. L., & Sivakoff, G. R. 2006, PASJ, 58, 131
- Gastaldello, F., Buote, D. A., Humphrey, P. J., et al. 2007, ApJ, 669, 158
- Gómez, P. L., Loken, C., Roettiger, K., & Burns, J. O. 2002, ApJ, 569, 122
- Heinz, S., Choi, Y.-Y., Reynolds, C. S., & Begelman, M. C. 2002, ApJ, 569, L79
- Heinz, S., Reynolds, C. S., & Begelman, M. C. 1998, ApJ, 501, 126
- Henriksen, M. J. & Markevitch, M. L. 1996, ApJ, 466, L79
- Henry, J. P. & Briel, U. G. 1995, ApJ, 443, L9
- Henry, J. P., Finoguenov, A., & Briel, U. G. 2004, ApJ, 615, 181
- Huang, Z. & Sarazin, C. L. 1998, ApJ, 496, 728
- Ikebe, Y., Reiprich, T. H., Böhringer, H., Tanaka, Y., & Kitayama, T. 2002, A&A, 383, 773
- Jones, C. & Forman, W. 1984, ApJ, 276, 38
- Kassim, N. E., Clarke, T. E., Enßlin, T. A., Cohen, A. S., & Neumann, D. M. 2001, ApJ, 559, 785
- Kawano, N., Fukazawa, Y., Nishino, S., et al. 2008, ArXiv:0805.3582
- Kempner, J. C., Sarazin, C. L., & Ricker, P. M. 2002, ApJ, 579, 236
- Laganá, T. F., Lima Neto, G. B., Andrade-Santos, F., & Cypriano, E. S. 2008, A&A, 485, 633
- Lima Neto, G. B., Pislar, V., & Bagchi, J. 2001, A&A, 368, 440
- Liuzzo, E., Giovannini, G., & Giroletti, M. 2009, ArXiv:0903.0812
- Markevitch, M., Mazzotta, P., Vikhlinin, A., et al. 2003, ApJ, 586, L19
- Markevitch, M., Sarazin, C. L., & Vikhlinin, A. 1999, ApJ, 521, 526
- Markevitch, M. & Vikhlinin, A. 2007, Phys. Rep., 443, 1
- Matsuzawa, H., Matsuoka, M., Ikebe, Y., Mihara, T., & Yamashita, K. 1996, PASJ, 48, 565
- McNamara, B. R., Nulsen, P. E. J., Wise, M. W., et al. 2005, Nature, 433, 45
- McNamara, B. R., Wise, M., Nulsen, P. E. J., et al. 2000, ApJ, 534, L135
- Nulsen, P. E. J., McNamara, B. R., Wise, M. W., & David, L. P. 2005, ApJ, 628, 629
- Owers, M. S., Couch, W. J., & Nulsen, P. E. J. 2009a, ApJ, 693, 901
- Owers, M. S., Nulsen, P. E. J., Couch, W. J., Markevitch, M., & Poole, G. B. 2009b, ApJ, 692, 702
- Poole, G. B., Fardal, M. A., Babul, A., et al. 2006, MNRAS, 373, 881
- Proust, D., Mazure, A., Sodre, L., Capelato, H., & Lund, G. 1988, A&AS, 72, 415
- Randall, S. W., Jones, C., Markevitch, M., et al. 2009,

- ArXiv:0904.0610
- Reiprich, T. H., Sarazin, C. L., Kempner, J. C., & Tittley, E. 2004, *ApJ*, 608, 179
- Reynolds, C. S., Casper, E. A., & Heinz, S. 2008, *ApJ*, 679, 1181
- Reynolds, C. S., Heinz, S., & Begelman, M. C. 2001, *ApJ*, 549, L179
- Rottgering, H. J. A., Wieringa, M. H., Hunstead, R. W., & Ekers, R. D. 1997, *MNRAS*, 290, 577
- Sanders, J. S. & Fabian, A. C. 2006, *MNRAS*, 371, 1483
- Sanders, J. S. & Fabian, A. C. 2008, *MNRAS*, 390, L93
- Sharma, M., McNamara, B. R., Nulsen, P. E. J., et al. 2004, *ApJ*, 613, 180
- Taylor, G. B., Barton, E. J., & Ge, J. 1994, *AJ*, 107, 1942
- Taylor, G. B., Fabian, A. C., & Allen, S. W. 2002, *MNRAS*, 334, 769
- Vernaleo, J. C. & Reynolds, C. S. 2006, *ApJ*, 645, 83
- Watanabe, M., Yamashita, K., Furuzawa, A., Kunieda, H., & Tawara, Y. 2001, *PASJ*, 53, 605
- Wise, M. W., McNamara, B. R., Nulsen, P. E. J., Houck, J. C., & David, L. P. 2007, *ApJ*, 659, 1153
- Zappacosta, L., Buote, D. A., Gastaldello, F., et al. 2006, *ApJ*, 650, 777
- Zhao, J.-H., Sumi, D. M., Burns, J. O., & Duric, N. 1993, *ApJ*, 416, 51